

1 **Cr(VI) removal from aqueous solution using a magnetite snail shell**

2  
3  
4  
5  
6  
7  
8  
9  
10  
11  
12  
13  
14  
15  
16  
17  
18  
19  
20  
21  
22  
23  
24  
25  
26  
27  
28  
29  
30  
31  
32  
33  
34  
35  
36  
37  
38  
39

Le Phuong Hoang

Faculty of Civil and Environmental Engineering, Thai Nguyen University of Technology (TNUT), TichLuong Ward,  
Thai Nguyen, Vietnam.

Thi Minh Phuong Nguyen

Faculty of Environment and Chemical Engineering, Duy Tan University (DTU), 254 Nguyen Van Linh road, Da  
Nang, Vietnam.

Huu Tap Van

Faculty of Natural Resources and Environment, Thai Nguyen University of Sciences (TNUS), Tan Thinh ward, Thai  
Nguyen, Vietnam.

Thi Kim Dung Hoang

Faculty of Civil and Environmental Engineering, Thai Nguyen University of Technology (TNUT), TichLuong Ward,  
Thai Nguyen, Vietnam.

Xuan Hoa Vu

Institute of Research and Development, Duy Tan University, Da Nang 550000, Vietnam.

Tien Vinh Nguyen

Faculty of Engineering and IT, University of Technology Sydney (UTS), Box 123, Broadway, Sydney, PO,  
Australia.

N.X. Ca

Laboratory of Advanced Materials Chemistry, Advanced Institute of Materials Science, Ton Duc Thang University,  
Ho Chi Minh City, Vietnam

Faculty of Applied Sciences, Ton Duc Thang University, Ho Chi Minh City, Vietnam

Corresponding author: Email: [nguyexuanca@tdtu.edu.vn](mailto:nguyexuanca@tdtu.edu.vn)

## 40 Abstract

41 In this study, magnetic snail shell (MSS) prepared by impregnating of iron oxide onto snail shell (SS) powder was  
42 used for removing Cr(VI) from aqueous solution. Among 6 different mass ratios of Fe/SS powder studied, the  
43 MSS25 produced at a ratio of 25% achieved the highest Cr(VI) adsorption capacity. Batch adsorption experiments  
44 were conducted to investigate the adsorption isotherm, kinetics and mechanism of Cr(VI) onto MSS25. The results  
45 illustrated that adsorption of Cr(VI) onto MSS25 reached equilibrium after 150 min at pH 3. The adsorption kinetics  
46 could be well described by the pseudo-second order model ( $R^2=0.986$ ). The Langmuir model ( $R^2=0.971$ ) was the  
47 best-fitting model that described the adsorption isotherm of Cr(VI) onto MSS25. The maximum adsorption capacity  
48 was 46.08 mg Cr(VI) per gram of MSS25. Ion-exchange, electrostatic attraction and adsorption-coupled reduction  
49 were determined as the main adsorption mechanisms of Cr(VI) onto MSS25. The high percentages of  $\text{CaCO}_3$  and  
50  $\text{Fe}_3\text{O}_4$  found in the MSS25 structure made a significant contribution to the Cr(VI) adsorption process.

**Keywords:** Cr(V) removal, magnetic snail shell, adsorption, low-cost adsorbent

51  
52 **1. Introduction**  
53 The discharge of industrial wastewater containing toxic heavy metals into the natural environment is one of the  
54 world's most serious pollution issues. Hexavalent chromium (Cr(VI)) is one of the most toxic heavy metals and has a  
55 lethal dose of only 0.1 mg/kg body weight. Drinking Cr(VI) contaminated water can lead to serious problems such as  
56 liver damage and pulmonary congestion (Karimi et al. 2012). Cr(VI) often exists in the effluents of industrial  
57 processes such as electroplating, leather tanning, textiles, mining, metallurgy and making fertilizer (Zhou et al.  
58 2016). Therefore, it is necessary to remove Cr(VI) from wastewater before discharging it into the natural  
59 environment. Several technologies to remove Cr(VI) from industrial wastewaters have been reported such as ion  
60 exchange, electrolytic removal, adsorption, chemical precipitation, membrane filtration and solvent extraction  
61 (Bhaumik et al. 2013). Adsorption has been considered one of the most attractive methods due to its cost  
62 effectiveness, simplicity of operation and high removal efficiency, even when contaminants are in small  
63 concentrations in water environments (Mthombeni et al. 2018). Researchers have tried to find adsorbents which are  
64 low cost and have high adsorption capacity. Many natural adsorbents such as agricultural by-products (peanut hull,  
65 corncob, rice straw, walnut hull and mango kernel) (Inyang et al. 2016; Rai et al. 2016), biomass (*Spirulina maxima*  
66 and *Rhizopusnigricans*) (Bai R and Abraham 2001; Gong et al. 2005), and natural ore (zeolite; kaolinite)  
67 (Mthombeni et al. 2015; Turan et al. 2007) have been studied.

68 Biogenic calcium carbonate has been trialed successfully as a cost-effective biosorbent for heavy metals removal (Du  
69 et al. 2011; Hossain and Aditya 2013). Freshwater snail and mussel shells include 95%–99% calcite and/or aragonite  
70 (Hossain et al. 2015). They can be considered as potential cost-effective biosorbents due to their high calcium  
71 carbonate content. Some authors reported that their shell dust could effectively adsorb toxic metals (Du et al. 2011;  
72 Hossain and Aditya 2013; Van et al. 2018). The shell dust of the freshwater snail (*Lymnaeaaluteola*) can remove  
73 cadmium from aqueous solution with a high adsorption capacity of 16.66 mg/g being reported (Hossain and Aditya  
74 2013). Mollusk shell powder was also documented for its effective removal of Pb, Cd and Zn from aqueous solutions  
75 with the epitaxial growth of otavite crystal on the surface of calcite (Du et al. 2011). In Vietnam and many countries  
76 in Asia, fresh snail is a very popular food source. A large amount of fresh snail shell is directly discharged into the

77 environment, which then causes odor issues. A new biosorbent produced from used snail shell can be an economical  
78 solution to: firstly, environmental pollution caused by heavy metals in aqueous environments; and secondly, manage  
79 used snail shells for other practical applications.

80 Recently, magnetic adsorbents have attracted more scientific attention due to their effective absorptivity and easy  
81 recovery of used materials after the treatment process (Han et al. 2016). These magnetic adsorbents can be  
82 synthesized by impregnating iron onto different materials such as biochar (Shang et al. 2016), activated carbon (Hao,  
83 Wang, Yan, Jiang, & Xu, 2018) or biomass (Akram et al. 2017), etc. However, to the best of our knowledge, no study  
84 has been done on combining snail shell and iron to produce a new magnetic material for Cr(VI) removal from  
85 aqueous solution. The aim of this study, therefore, was to: (i) develop a new absorbent namely magnetic snail shell  
86 (MSS) by impregnating iron oxide onto freshwater snail shell powder; and (ii) evaluate the performance of MSS on  
87 removing Cr(VI) from aqueous solution. The batch experiments under various operational conditions (pH,  
88 impregnation ratio of Fe and snail shell powder, concentrations of MSS and Cr(VI), contact time) were carried out to  
89 understand the behaviors of Cr(VI) adsorption onto MSS and to identify the adsorption mechanisms.

90

## 91 **2. Materials and methods**

92

### 93 2.1. Chemicals

94

95 All chemicals used in this study ( $\text{FeCl}_3 \cdot 6\text{H}_2\text{O}$ ,  $\text{K}_2\text{Cr}_2\text{O}_7$ , HCl and NaOH) were purchased from Merck (Darmstadt,  
96 Germany). The Cr(VI) stock solution (1000 mg/L) was prepared by dissolving 0.7024 g of potassium dichromate  
97 ( $\text{K}_2\text{Cr}_2\text{O}_7$ ) in 250 mL double distilled water. Working Cr(VI) solutions with the desired concentrations were obtained  
98 by diluting the stock solution with double distilled water.

99

### 100 2.2. Preparation of magnetic snail shell

101

102 Snail shell (*Bellamyachinensis*) (SS) was collected from local restaurants in Thai Nguyen province, Vietnam. Snail  
103 shell was washed several times with tap water and distilled water to remove any adhering tissue portions. After  
104 cleaning with water, SS samples were air-dried (under sunlight) and then soaked in 0.1 M sulfuric acid solution for  
105 8h and washed again with distilled water to remove any residual acid. The clean SS was then dried at  $100^\circ\text{C}$  for 48h  
106 before it was crushed and sieved to a particle size of  $\leq 0.5$  mm for further experimentation.

107 Magnetic snail shell (MSS) was prepared according to the method employed by He et al. (2018) as follows. A  
108 predetermined amount of clean SS powder was soaked into the  $\text{FeCl}_3$  solution of 100 g Fe/L with different mass  
109 ratios of Fe/SS powder, these being 0%, 5%, 10%, 15%, 20%, 25% and 30% (w/w). After agitating for 2h using  
110 magnetic stirrers, the mixtures were dried at  $80^\circ\text{C}$ . The final dried products were marked as MSS0, MSS5, MSS10,  
111 MSS15, MSS20, MSS25 and MSS30, respectively, and stored in sealed bags before testing. MSS25 presented the  
112 best performance (details are presented in section 3.1) and so was chosen for the detailed characterization and batch  
113 experiments.

114

### 115 2.3. Characterization of magnetic snail shell

116

117 The morphological characteristics of clean SS, new MSS and MSS after absorption of Cr(VI) (MSS25-Cr) were  
118 determined by an energy dispersive X-ray spectroscopy equipped with EDS and SEM system (HITACHI S-4800),  
119 X-ray diffraction XRD-D8 ADVANCE with the Cu Ka radiation ( $\lambda = 1.54 \text{ \AA}$ ). The functional groups of SS, MSS25  
120 and Cr-MSS25 were identified by Fourier transform infrared spectroscopy (FTIR-6300) in the 500–4000  $\text{cm}^{-1}$  range.  
121 The surface area ( $S_{\text{BET}}$ ) of SS and MSS25 was determined by nitrogen adsorption/desorption isotherm at 77.35<sup>0</sup>K  
122 (Coulter, USA).  $\text{pH}_{\text{PZC}}$  was determined via the common pH drift method (Zhao et al. 2016).

123

#### 124 2.4. Batch adsorption experiments

125

126 Batch model experiment was conducted to evaluate the adsorption behavior of Cr(VI) on SS and MSS25 at different  
127 conditions, including impregnation ratio of Fe/SS (w/w) (0%, 5%, 10%, 15%, 20% and 25%), pH (2-12), contact  
128 time (5-240 min), adsorbent dose (10-120 mg/25 mL), and initial Cr(VI) concentration (5–80 mg/L). Batch  
129 experiments were conducted utilizing 50 mL Erlenmeyer flasks containing 25 mL of Cr(VI) solution. The initial pH  
130 of Cr(VI) solution was adjusted to a predetermined value by using HCl 0,1 M and NaOH 0,1M. The flasks were  
131 covered by paraffin before agitating them at 120rpm with a shaker (PH-2A, China). After the adsorption, the  
132 adsorbent-adsorbate mixture was separated by Whatman No. 1 filter papers (pore size of 11  $\mu\text{m}$ ). The total  
133 concentration of Cr(VI) remaining in the solution was determined by using Inductively coupled plasma-optical  
134 emission spectrometry (ICP-OES, Model: ULTIMA EXPERT, Horiba, France). The Cr(VI) amounts adsorbed onto  
135 MSS25 at any time  $t$  ( $q_t$ , mg/g) and equilibrium ( $q_e$ , mg/g) were calculated by equations 1 and 2:

$$136 \quad q_t = \frac{(C_0 - C_t)V}{M} \quad (1)$$

137 where:  $C_0$ ,  $C_t$  and  $C_e$  (mg/L) are concentrations of Cr(VI) in solution at the start, any time  $t$ , and equilibrium,  
138 respectively;  $V$  (L) is the volume of solution and  $M$  (g) is the dry weight of used adsorbent.

#### 139 2.5. Adsorption kinetics

140 The pseudo-first-order, pseudo-second-order and Elovich models were used to analyze the experimental data in the  
141 kinetics study. The linear form of these three popular models can be written as follows, respectively:

$$142 \quad \ln(q_e - q_t) = \ln q_e - k_1 t \quad (2)$$

$$143 \quad \frac{t}{q_t} = \frac{1}{k_2 q_e^2} + \frac{1}{q_e} t \quad (3)$$

$$144 \quad q_t = \beta \ln(\alpha \beta t) \quad (4)$$

145 where:  $q_t$  (mg/g) and  $q_e$  (mg/g) is the adsorption capacity at time  $t$  (min) and at equilibrium, respectively;  $k_1$  (1/min)  
146 and  $k_2$  (g/mg.min) are the rate constant of the pseudo-first-order and pseudo-second-order models, respectively;  $\alpha$   
147 (mg/g.min) is the initial adsorption rate;  $\beta$  (g/mg) is the adsorption constant.

148

#### 149 2.6. Adsorption isotherm models

150 The adsorption isotherm equilibrium provides useful data for explaining the adsorption mechanism. In this study,  
151 three adsorption isotherm models Langmuir, Freundlich and Temkin- were employed. The equations for these  
152 models are described below by Eqs (6), (7) and (8), respectively:

$$153 \quad q_e = \frac{q_m K_L C_e}{1 + K_L C_e} \quad (5)$$

154  $q_e = K_F C_e^{\frac{1}{n}}$  (6)

155  $q_e = \frac{RT}{b} \ln(A_T C_e)$  (7)

156 where:  $q_m$ (mg/g) is the maximum adsorption capacity,  $C_e$ (mg/L) and  $q_e$  (mg/g) are the concentration of Cr(VI) in  
 157 solution and adsorption capacity at equilibrium, respectively;  $K_L$ (L/mg): Langmuir constant;  $K_F$ (mg/g):Freundlich  
 158 constant;  $n$  is the adsorption intensity;  $A_T$  (L/g): Temkin isotherm equilibrium binding constant;  $b$ : Temkin isotherm  
 159 constant,  $R$  (8.314J/mol/K): universal gas constant;  $T$ : temperature at 298K.

160  
161

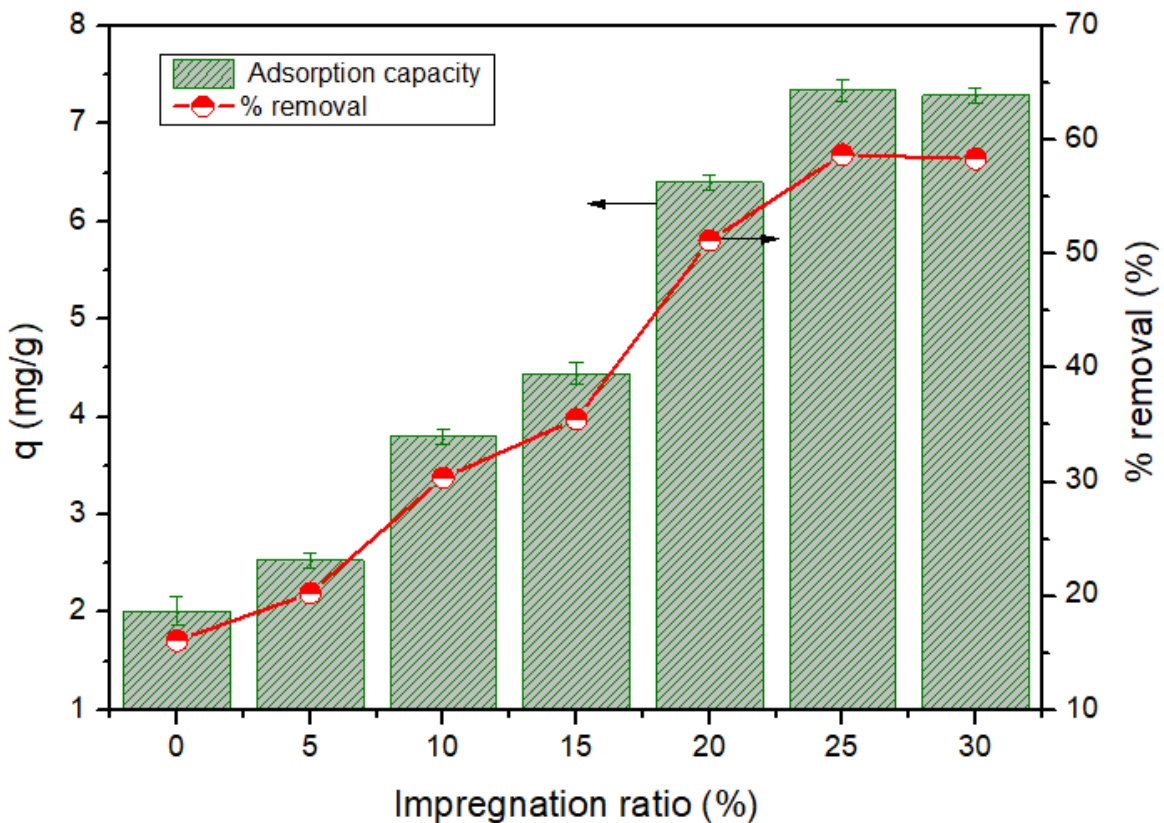
162 **3. Results and discussion**

163

164 3.1. Optimizing the impregnation ratio of Fe and snail shell powder to produce MSS25

165

166 The first set of experiments was conducted by mixing 20 mg of MSS25 produced at different ratios of Fe and snail  
 167 shell with 25 mL Cr(VI) solution of 10 mg/L at room temperature ( $25 \pm 2^\circ\text{C}$ ). The amounts of Cr(VI) adsorbed by  
 168 different magnetite SS are presented in Fig. 1.



169

170 **Fig. 1** The effect of the impregnation ratios of Fe/SS on Cr(VI) removal of MSS; Experimental conditions: initial  
 171 Cr(VI) concentration: 10 mg/L, adsorbent dose: 20 mg/25 mL solution, contact time: 60 min

172

173 Results from Fig. 1 show that Cr(VI) adsorption capacity ( $q$ ) and removal efficiency of MSS25 were higher than that  
 174 of other MSS. The increase in the impregnation ratios of Fe and SS from 0 to 25% led to substantial improvements in

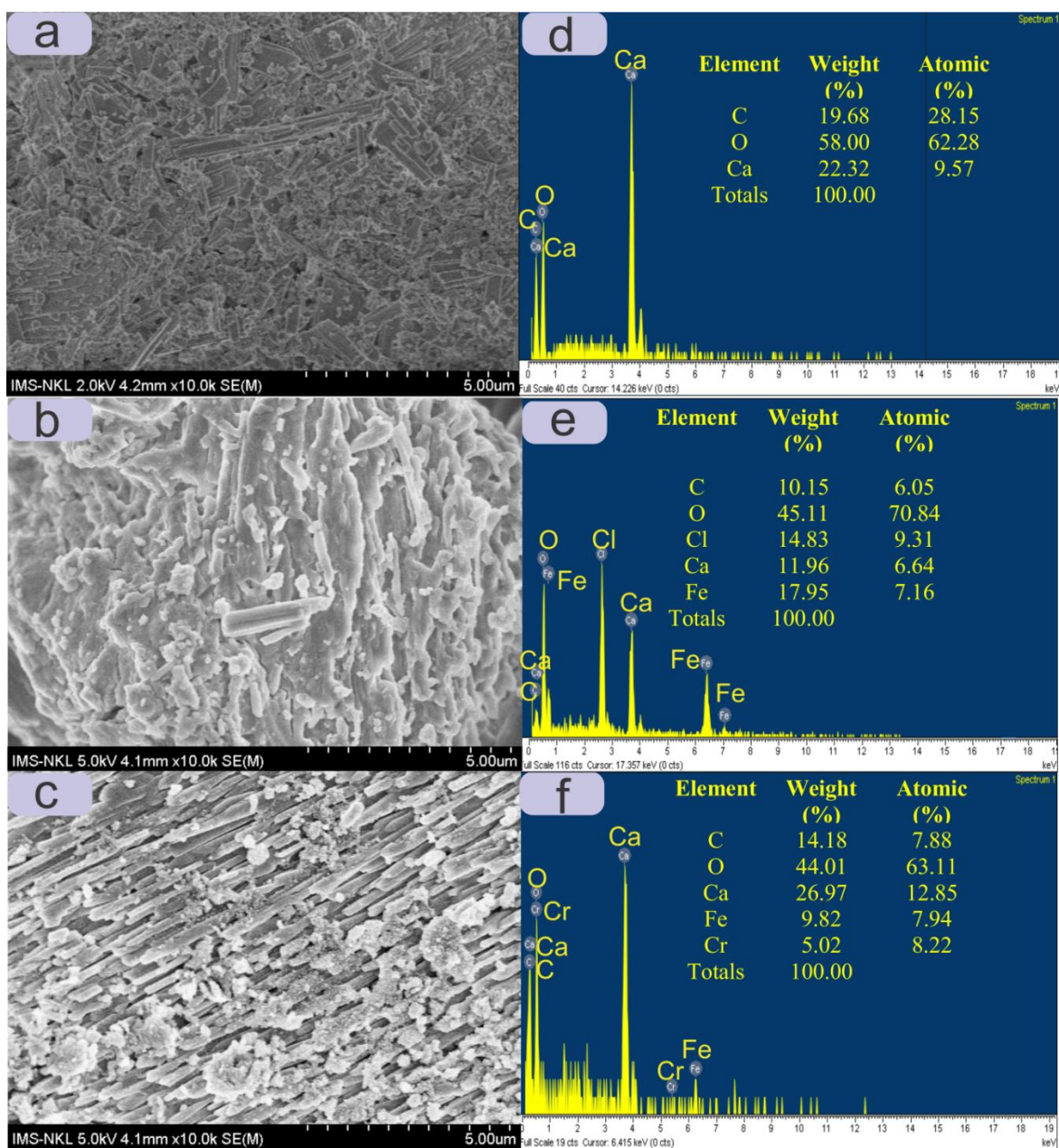
175 Cr(VI) adsorption capacity and removal efficiency, i.e. from 2.01 mg/g to 7.34 mg/g and from 16.07% to 58.73%,  
176 respectively. Lu et al. (2018) reported that Fe<sub>3</sub>O<sub>4</sub> particles in the adsorbent could form outer-sphere complexes with  
177 Cr(VI) and reduced Cr(VI) to Cr(III). However, when increase the impregnation ratio of Fe in SS to 30%, the  
178 removal efficiency of Cr(VI) only increased slightly to 58.93%. The trend of this result is similar to that of recent  
179 study of He et al. (2018). Their results indicate that Fe-impregnated biochar produced at a ratio of 30% did not  
180 significantly increase As removal efficiency compared to that produced at a ratio of 20%. Considering performance  
181 and economic factors, MSS25 produced at a Fe/SS ratio of 25% w/w was chosen for the subsequent experiments.

182

### 183 3.2. Characteristics of adsorbent

184

185 The BET surface area ( $S_{\text{BET}}$ ) and total pore volume of SS were smaller than 2 m<sup>2</sup>/g and 0.001 cm<sup>3</sup>/g, respectively.  
186 After modification, both  $S_{\text{BET}}$  and total pore volume of MSS25 increased significantly to 69.69 m<sup>2</sup>/g and 0.104  
187 cm<sup>3</sup>/g, respectively. The surface morphology and element composition of these adsorbents were shown in the results  
188 of SEM and EDS analyses. MSS25 possessed a more porous and rougher structure (Fig. 2b) than that of SS (Fig. 2a).  
189 Iron particles reacted with carbonate calcium (CaCO<sub>3</sub>) led to the release of carbon elements and change in structure  
190 of the snail shell. Therefore, MSS25 was more porous and rougher structure than that of SS. This illustrates that iron  
191 oxide was successfully onto biochar's surface and caused a significant increase in surface are and pore volume (He et  
192 al. 2018). The EDS analysis results (Fig. 2d) indicated that SS was mainly composed of C (28.15%), O (62.28%) and  
193 Ca (9.57%) elements which revealed that the SS were mainly composed of crystalline CaCO<sub>3</sub> (Van et al. 2018).  
194 However, Fig. 2e depicts the proportions of elements for C, O, Cl, Ca and Fe in MSS25 were 6.05%, 70.84%,  
195 9.31%, 6.64% and 7.16%, respectively. This indicated that iron oxide was successfully attached on SS's surface and  
196 this impregnation caused the difference between the surface of SS and MSS25. After MSS25 was used to adsorb  
197 Cr(VI) in solution, the Cr peaks appeared in the used MSS25 (Fig. 2f) and the surface morphology of MSS25-Cr was  
198 changed clearly (Fig. 2c). This clearly indicated the adsorption of Cr(VI) on the surface of MSS25.



199  
 200 **Fig. 2** SEM and EDS of (a, d)-snail shell (SS), (b, e)-magnetic snail shell (MSS25) and (c, f)-magnetic snail shell  
 201 after Cr(VI) adsorption (MSS25-25)

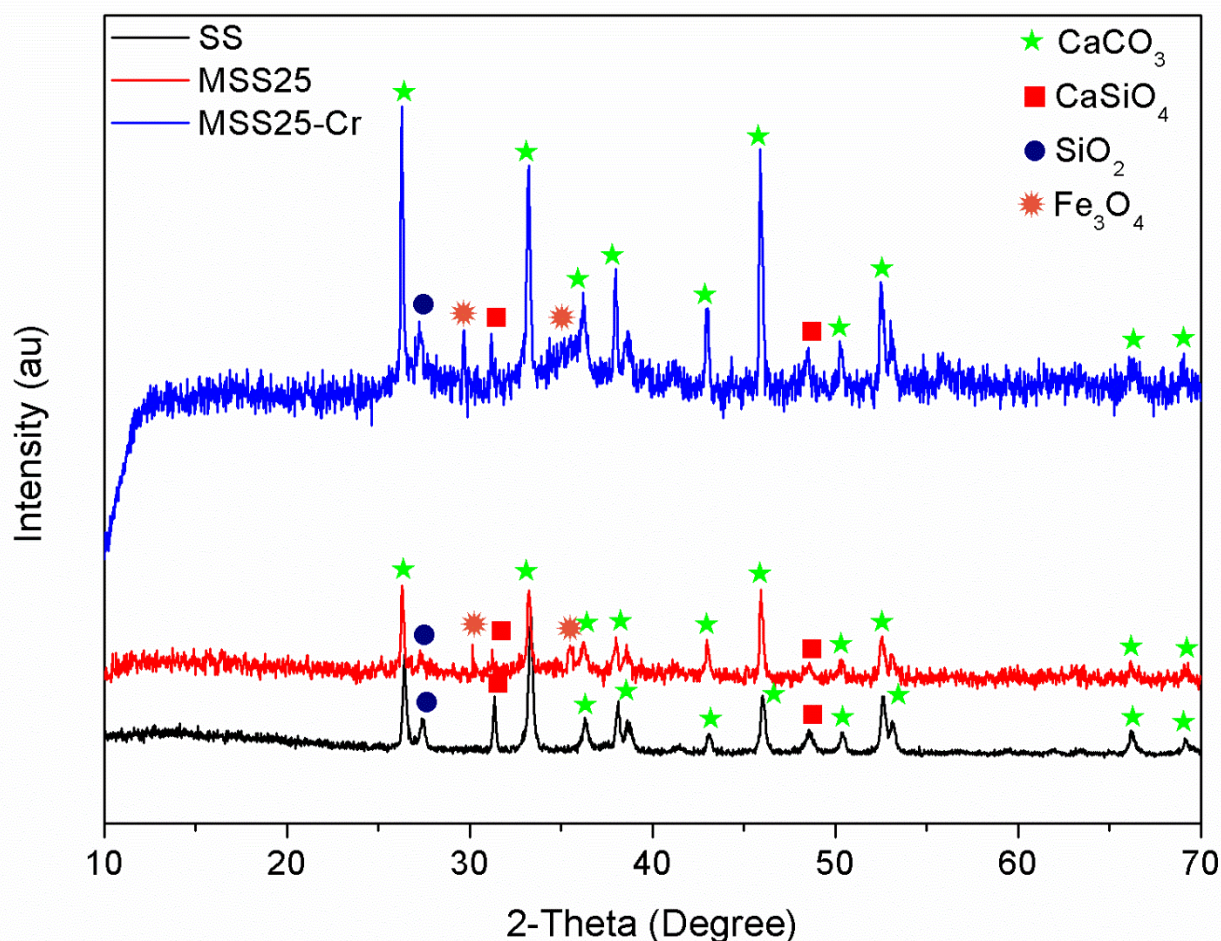
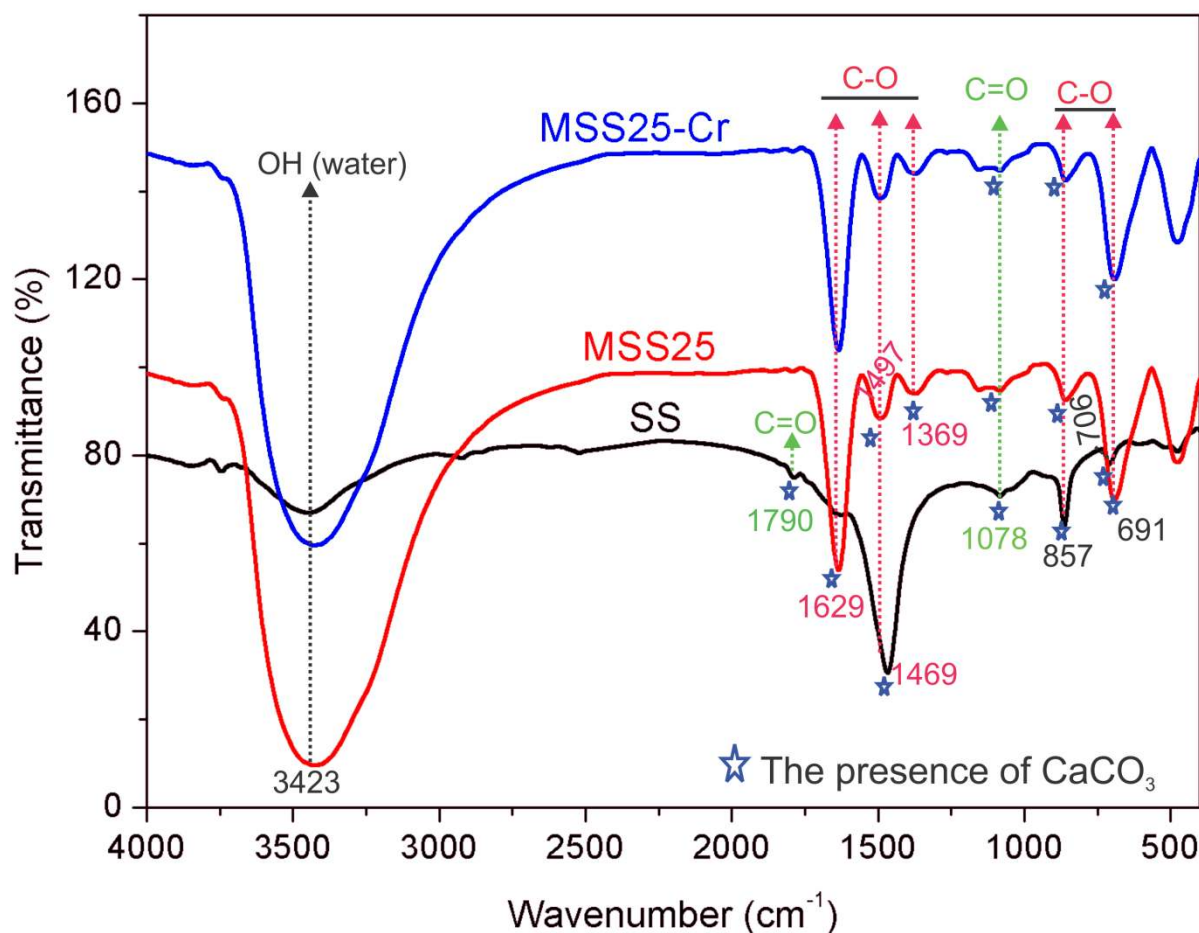


**Fig. 3** XRD graphs of snail shell (SS), magnetic snail shell (MSS25) and magnetic snail shell after Cr(VI) adsorption (MSS25-Cr)

202  
 203  
 204  
 205  
 206 The XRD data also confirmed the presence of large amounts of  $\text{CaCO}_3$  in SS. It suggests that SS is a biogenic  
 207 aragonite (Fig. 4). In XRD patterns of MSS25, the appearance of new peaks at  $30.0^\circ$ ,  $35.5^\circ$  and  $63.1^\circ$  were assigned  
 208 as  $\text{Fe}_3\text{O}_4$ , respectively (Hu et al. 2017; Lu et al. 2018). These results further confirmed that  $\text{Fe}_3\text{O}_4$  was successfully  
 209 formed onto MSS25. Moreover, the dominant functional groups on the SS, MSS25 and MSS25-Cr surfaces were  
 210 identified by the FTIR spectra (Fig. 4). A broad peak at around  $3423\text{ cm}^{-1}$  was assigned to the vibration of O–H  
 211 stretching. These peaks at approximately  $1629\text{ cm}^{-1}$ ,  $1469\text{ cm}^{-1}$ ,  $1497\text{ cm}^{-1}$ ,  $857\text{ cm}^{-1}$  and  $691\text{ cm}^{-1}$  contributed to the  
 212 carbonate group's C–O stretching vibration (Van et al. 2018; Tizo et al. 2018). The characteristic bands at  $1790\text{ cm}^{-1}$   
 213 and  $1078\text{ cm}^{-1}$  involved the stretching vibration of C=O groups of carbonate ion (Nan et al. 2008; Tizo et al. 2018).  
 214 This further confirms that calcite is the major constituent of SS powders. FTIR spectra of MSS25 and MSS25-Cr  
 215 presented two new peaks at  $1629\text{ cm}^{-1}$  and  $1369\text{ cm}^{-1}$  in comparison with that of SS. Moreover, the peaks at  $3423\text{ cm}^{-1}$   
 216  $^1$  and  $691\text{ cm}^{-1}$  became larger while the peak at  $1497\text{ cm}^{-1}$  was narrower than that in SS.





217  
 218 **Fig. 4** FTIR graphs of snail shell (SS), magnetic snail shell (MSS25) and magnetic snail shell after Cr(VI) absorption  
 219 (MSS25-Cr)  
 220

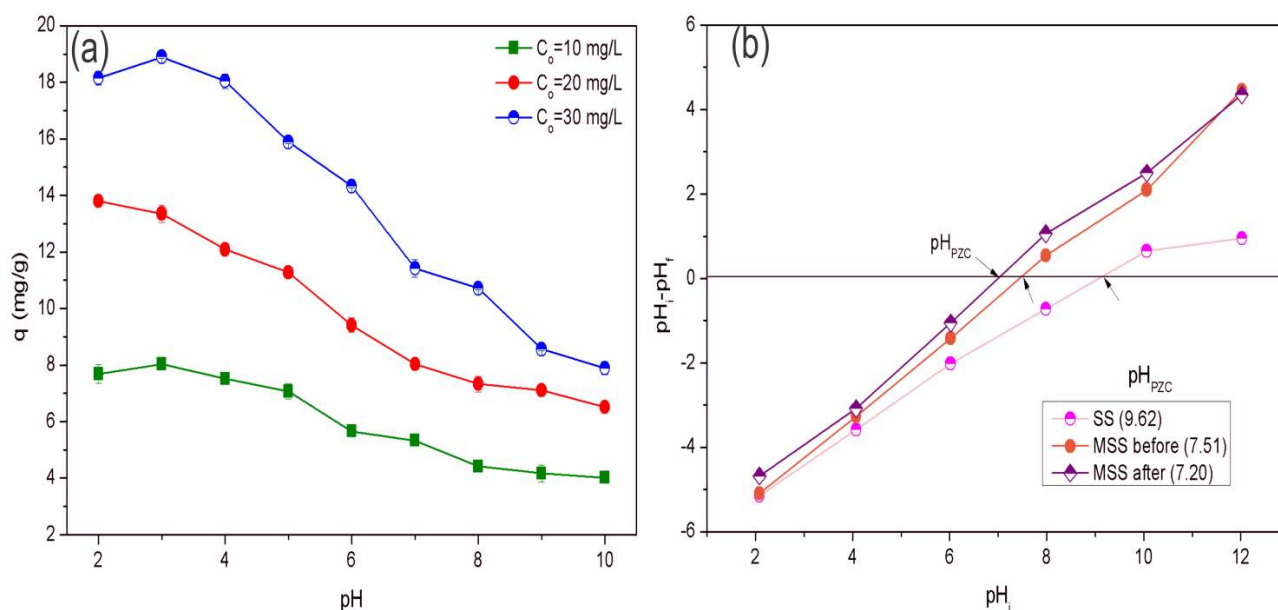
221 3.3 Effects of adsorption conditions on MSS25 performance

222  
 223 3.3.1. Effect of solution pH  
 224

225 The effect of pH of initial solution on Cr(VI) adsorption of MSS25 was investigated at different pH values, ranging  
 226 from 2.0 to 10.0. The experiment was carried out at initial Cr(VI) concentrations of 10 mg/L, 20 mg/L and 30 mg/L,  
 227 MSS25 dosage of 20 mg/25 mL solution and contact time of 60 min at room temperature ( $25 \pm 2^\circ\text{C}$ ). The  
 228 experimental results are shown in Fig. 5a. It can be seen that adsorption capacity of Cr(VI) onto MSS25 decreased  
 229 when solution pH increased. At pH from 2 to 3, the adsorption capacity of Cr(VI) reached the maximum values of  
 230 8.04 mg/g, 13.80 mg/g and 18.89 mg/g at initial Cr(VI) concentrations of 10 mg/L, 20 mg/L and 30 mg/L,  
 231 respectively. Meanwhile, the Cr(VI) adsorption decreased sharply when pH values increased from 4 to 10 in all three  
 232 initial Cr(VI) solutions. This decline can be explained as being due to: firstly, the effect of pH on the surface  
 233 properties of the adsorbent; and secondly, the forms of Cr ion in the solution (An et al. 2018; Chen et al. 2018; Zhou  
 234 et al. 2016). In acidic conditions, Cr(VI) can be easily reduced to Cr(III) which is adsorbed better than Cr(VI) (Wang  
 235 et al. 2014). As well, Cr(VI) mostly exists as  $\text{HCrO}_4^-$  and  $\text{Cr}_2\text{O}_7^{2-}$  at pH ranging from 2.0 to 6.4 and  $\text{CrO}_4^{2-}$  at pH > 6.4

236 (Chen et al. 2018; Zhou et al. 2016). The  $\text{HCrO}_4^-$  contains less adsorption free energy (-2.5 to -0.6 kcal/mol) than  
 237  $\text{CrO}_4^{2-}$  (-2.1 to -0.3 kcal/mol). Subsequently, in the same conditions,  $\text{CrO}_4^{2-}$  is more difficult to remove than  $\text{HCrO}_4^-$   
 238 (Shang et al. 2016).

239 Moreover, the zero point of charge ( $\text{pH}_{\text{PZC}}$ ) of MSS25 was 7.51 (Fig. 5b). It means that when  $\text{pH} < \text{pH}_{\text{PZC}}$  (7.51), the  
 240 surface of MSS25 was positively charged. This created significant electrostatic attraction with negatively charged  
 241 chromate forms in the solution (Chen et al. 2018). Conversely, when  $\text{pH} > \text{pH}_{\text{PZC}}$  (7.51), the surface of MSS25 was  
 242 negatively charged which hindered electrostatic force between the adsorbate and adsorbent (Akram et al. 2017). In  
 243 addition, an increase in the solution pH led to an increase in the  $\text{OH}^-$  which could then compete with  $\text{CrO}_4^{2-}$  to  
 244 occupy the active sites of MSS25 (Yang et al. 2018). Similar results have been reported in other studies (Akram et al.  
 245 2017; Shang et al. 2016). The results reported by Shang et al. (2016) showed that the maximum Cr(IV) adsorption  
 246 onto biochar derived from herb-residue was achieved at pH 2. The optimal pH for the adsorption of Cr(VI) onto bio-  
 247 composite of mango was reported at pH 3 (Akram et al. 2017).

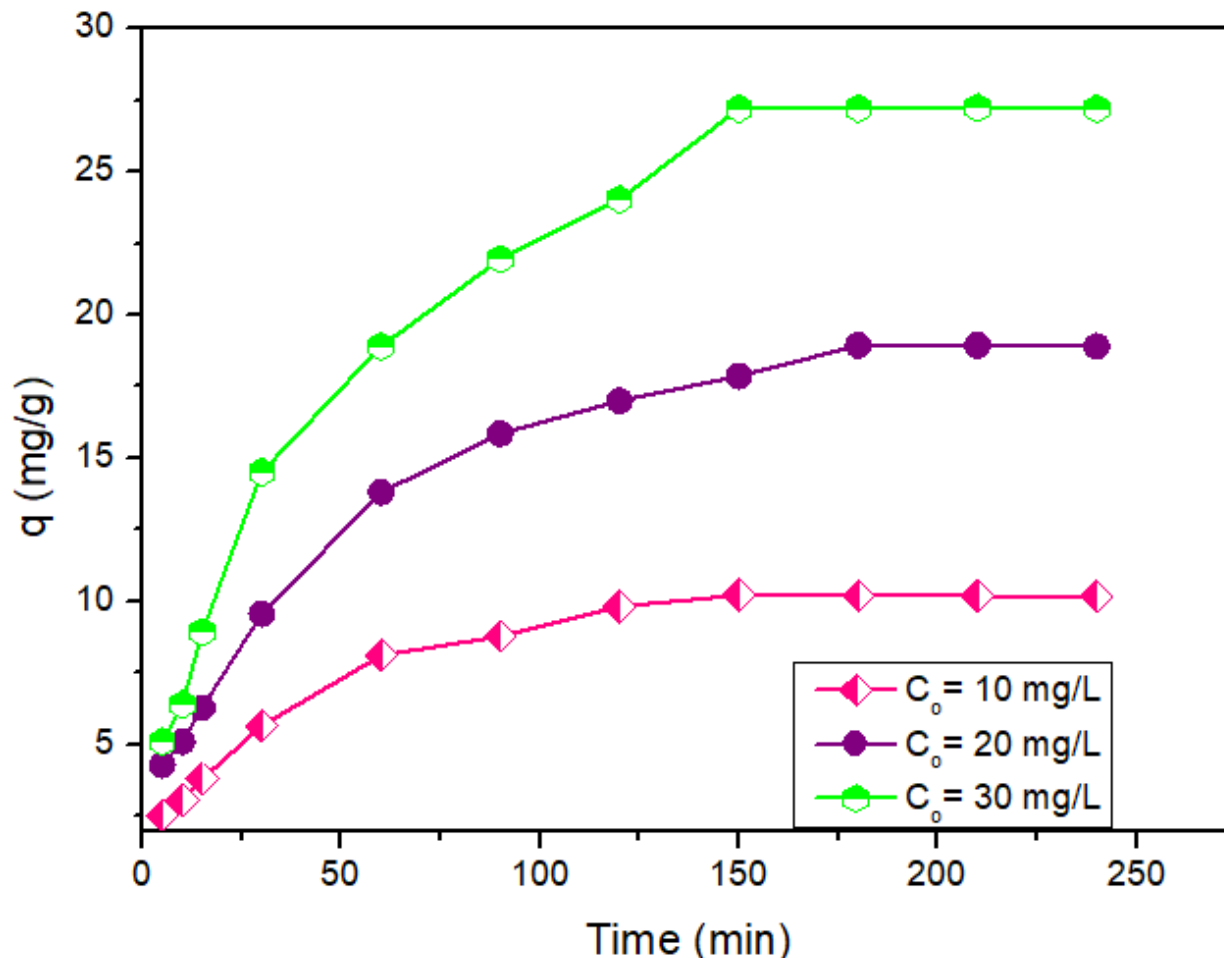


248 **Fig. 5** (a) Effect of pH on the adsorption capacity of Cr(VI) onto MSS25 and (b)  $\text{pH}_{\text{PZC}}$  of MSS25. Experimental  
 249 conditions: initial Cr(VI) concentrations: 10 mg/L, 20 mg/L and 30 mg/L; contact time: 60 min, adsorbent dose: 20  
 250 mg/25 mL  
 251  
 252

### 253 3.3.2. Effect of contact time

254  
 255 The effect of contact time on Cr(VI) adsorption was investigated at initial Cr(VI) concentrations of 10 mg/L, 20  
 256 mg/L and 30 mg/L, pH of 3.0, adsorbent dose of 20 mg/25 mL solution and contact time ranging from 5 to 240 min.  
 257 Fig. 6 shows that for the first 150 min, the Cr(VI) adsorbed onto MSS25 increased significantly, from 2.53 to 10.21  
 258 mg/g, 4.27 to 17.85 mg/g and 5.09 to 27.20 mg/g at initial Cr(VI) concentrations of 10 mg/L, 20 mg/L and 30 mg/L,  
 259 respectively. The reason for this phenomenon is that a large number of active sites on the surface of the adsorbent  
 260 was available at the beginning (Deveci and Kar 2013). By further increasing the contact time from 150 to 240 min,  
 261 the adsorbed amount increased slowly and remained unchanged due to the decline in the number of vacant sites

262 (Nguyen et al. 2019; Zhang et al. 2018). According to the results documented in this study, the contact time of 150  
 263 min was the best for removing Cr(VI) by MSS25 and therefore was used for the subsequent experiments. A similar  
 264 equilibrium time of 150 min was also reported in one study of Cr(VI) adsorption on activated carbon prepared from  
 265 mango kernel (Rai et al. 2016).

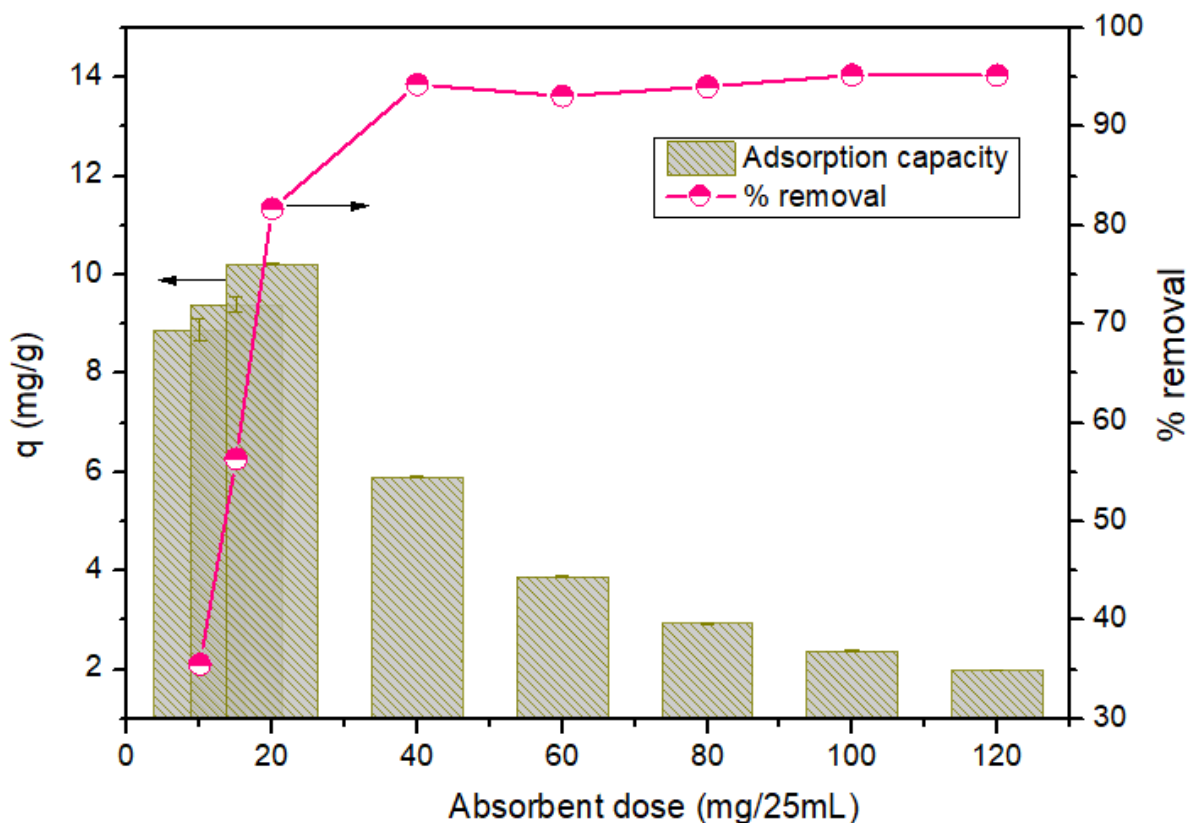


266  
 267 **Fig. 6** Effect of contact time on Cr(VI) adsorption by MSS25; Experimental conditions: initial Cr(VI) concentration:  
 268 10 mg/L, 20 mg/L, 30 mg/L; adsorbent dose: 20 mg/25 mL; pH: 3

269  
 270 3.3.3. Effect of adsorbent dose

271  
 272 Adsorbent concentration has been considered to be a significantly factor determined the adsorbent-adsorbate  
 273 equilibrium of the adsorption process (Deveci and Kar 2013; Xu et al. 2019). In this study, the dependence of Cr(VI)  
 274 adsorption on MSS25 doses was conducted with the amount of adsorbent ranging from 10 to 120 mg/25mL, solution  
 275 pH of 3, initial Cr(VI) concentration of 10 mg/L and contact time being 150 min. As seen in Fig. 7, the efficiency in  
 276 removing Cr(VI) rose significantly from 35.51% to 94.28% when the MSS25 dose increased from 10 to 40  
 277 mg/25mL. It can be explained that with the increase of adsorbent dose, the number of activate sites on FSS surface  
 278 also rose and led to an increase in the binding sites for complexation of chromium ions (Bai R and Abraham 2001;  
 279 Ertugay and Bayhan 2008). The experimental adsorption capacity reached the maximum value of 10.21 mg/g at the

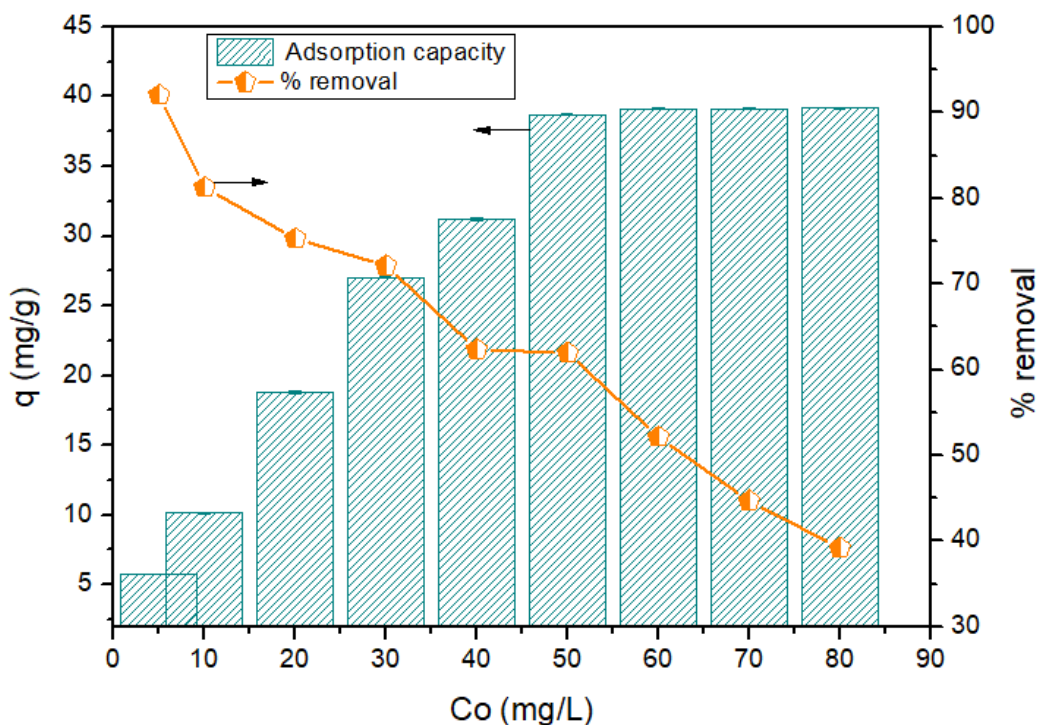
280 dose of 20 mg/25m. However, when increasing the adsorbent dose from 20 to 120 mg/25mL, the adsorption capacity  
281 fell sharply from 10.21 mg/g to 1.98 mg/g due to the overdose of adsorbent.



282  
283 **Fig. 7** Effect of adsorbent dosage on adsorption capacity and removal efficiency of Cr(VI) by MSS25; Experimental  
284 conditions: initial Cr(VI) concentration: 10 mg/L, contact time: 150 min, pH: 3

285  
286 3.3.4. Effect of initial Cr(VI) concentration

287  
288 The initial concentration is also an important factor in that it provides a vital driving force to overcome all mass  
289 transfer resistance of metal ion between the aqueous solution and adsorbent (Dönmez and Aksu 2002). The effect of  
290 initial Cr(VI) ions concentration from 5 to 80 mg/L was investigated and results are shown in Fig. 8. It can be  
291 observed that adsorption capacity of Cr(VI) onto MSS25 increased from 5.75 mg/g to 39.09 mg/g when increasing  
292 the initial Cr(VI) concentration from 5 to 60 mg/L. However, at initial Cr(VI) concentration of more than 60 mg/L,  
293 the adsorption capacity did not increase any further. On the other hand, the amount of Cr(VI) removed fell from  
294 92.03% to 39.17%, which corresponded to the increase of the initial Cr(VI) concentration from 5 to 80 mg/L. This  
295 can be explained by the increase of contact between activated sites on the adsorbent's surface with adsorbate. After a  
296 certain level of increase in the initial Cr(VI) concentration, the available sites were occupied and saturated. Thus  
297 adsorption capacity of Cr(VI) reached stability (Rai et al. 2016). In addition, the ratio of available activated sites to  
298 Cr(VI) ions was lower at higher Cr(VI) concentration (Bai R and Abraham 2001). Consequently, the Cr(VI) removal  
299 efficiency decreased at the higher concentration. A similar trend on the role of initial Cr(VI) concentration in the  
300 adsorption process has been reported elsewhere such as research on removal of Cr(VI) from aqueous solutions using  
301 wheat shell (P. Das Saha et al. 2012) or walnut hull (X. S. Wang et al. 2009).



302  
 303 **Fig. 8** Effect of initial Cr(VI) concentration on the adsorption capacity and removal efficiency when using MSS25;  
 304 Experimental conditions: solution pH: 3, contact time: 150 min, adsorbent dose: 20 mg/25mL  
 305

306 3.3.5. Adsorption kinetics

307 The linear fitting kinetic parameters are summarized in Table 1 and Fig. 9. The linear regression coefficient  $R^2$  values  
 308 in the pseudo-first-order model, pseudo-second-order model and Elovich model were 0.975, 0.986 and 0.971,  
 309 respectively. These results show that the Cr(VI) adsorption onto MSS25 fitted well with all three models. The  
 310 pseudo-second-order model obtained the highest  $R^2$  value. The calculated results of adsorption capacity derived from  
 311 the pseudo-second order models (11.72 mg/g) were also close to the experimental data ( $q_{e,exp}$  of 11.13 mg/g). This  
 312 indicated two things: firstly, the pseudo-second-order model was the best fit for Cr(VI) removal by MSS25. It also  
 313 indicated; and secondly, the adsorption of Cr(VI) onto MSS25 was a chemical sorption process.

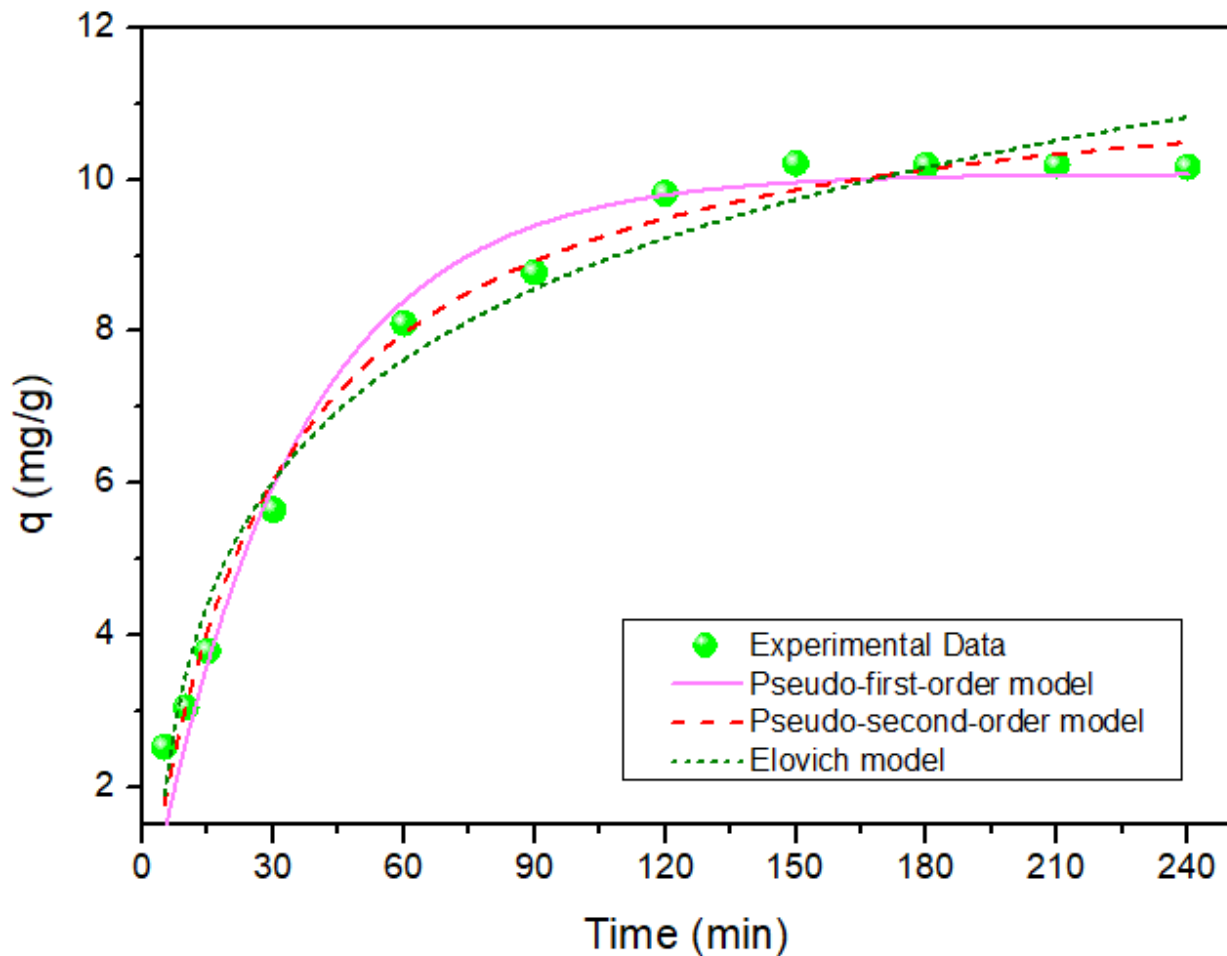
314

315 **Table 1.** Kinetics parameters of models on Cr(VI) adsorption by MSS25

Pseudo-first-order			Pseudo-second-order			Elovich			$q_{e, exp}$ (mg/g)
$q_{e, cal}$ (mg/g)	$k_1$	$R^2$	$q_{e, cal}$ (mg/g)	$k_2$	$R^2$	$\alpha$	$\beta$	$R^2$	
10.08	0.029	0.975	11.72	0.003	0.986	0.196	2.307	0.971	11.13

316

317



318  
 319 **Fig. 9** Kinetics models of Cr(VI) adsorption onto MSS25; Experimental conditions: initial Cr(VI) concentration: 10  
 320 mg/L; adsorbent dose: 20 mg/25 mL; pH: 3; contact time: 150 min  
 321

322 3.3.6. Adsorption isotherm

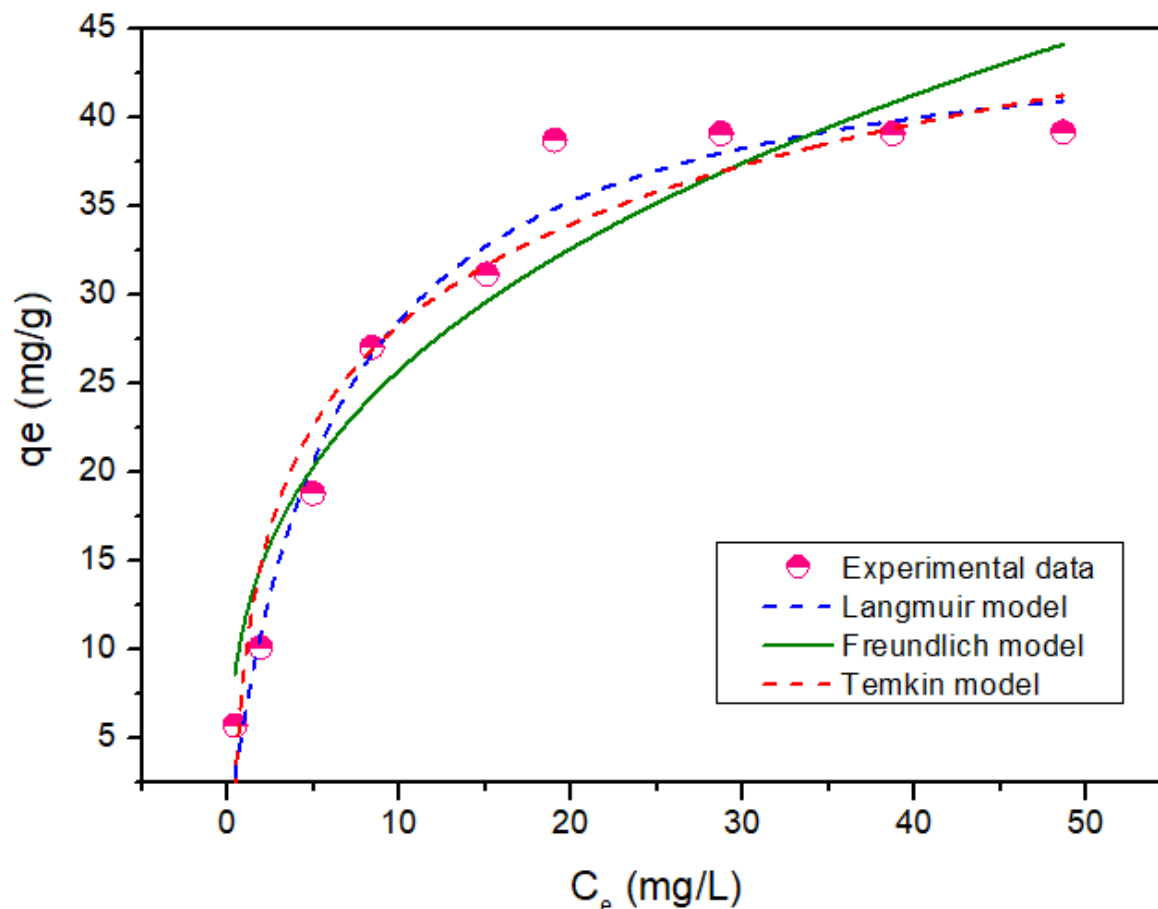
323 The data obtained by fitting the three models are listed in Table 2 and their plots are shown in Fig. 10. With the  
 324 highest  $R^2$  values (0.971) and the minor difference between calculated  $q_m$  value (46.08 mg/g) and  $q_{exp}$  (39.17 mg/g),  
 325 the Langmuir model is considered to be the best one for describing the adsorption of Cr(VI) onto MSS25. This  
 326 suggested that the adsorption mainly occurred in the monolayer or through a fixed number of identical sites on the  
 327 MSS25 surface. The adsorption also occurred at homogeneous adsorption sites of the MSS25 adsorbent (Shang et al.  
 328 2016). Furthermore, the  $1/n$  value (0.339) obtained from the Freundlich model was below 1, which meant that the  
 329 adsorption of Cr(VI) on MSS25 was favorable (Yuan et al. 2009).

330

331 **Table 2** The adsorption isothermal parameters of Cr(VI) onto MSS25

Langmuir model			Freundlich model			Temkin model			$q_{mexp}$ (mg/g)
$q_m$ (mg/g)	$K_L$	$R^2$	$K_F$	$1/n$	$R^2$	$A_T$	$b$	$R^2$	
46.08	0.163	0.971	11.790	0.339	0.904	34.749	304.725	0.931	39.17

332



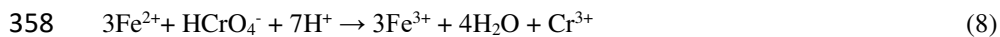
334  
 335 **Fig. 10** Adsorption isotherm of Cr(VI) onto MSS25; Experimental conditions: adsorbent dose: 20 mg/25 mL; pH: 3;  
 336 contact time: 150 min

337  
 338 3.3.7. Adsorption mechanism

339  
 340 The adsorption mechanism of toxic metals onto carbonate-rich materials was controlled by (1) pore filling, (2)  
 341 electrostatic attraction (out-sphere complexes), (3) non-electrostatic attraction (inner-sphere complexation), (4)  
 342 surface precipitation and (5) cation exchange (Alidoust et al. 2015). In this study, the adsorption mechanisms of  
 343 Cr(VI) were also affected by the surface properties of MSS25. As previously discussed, the MSS25 adsorbent  
 344 exhibited a higher  $S_{BET}$  value (69.69  $m^2/g$ ) than SS (< 2  $m^2/g$ ). Moreover, the analyses on the effects of pH show that  
 345 the main adsorption of Cr(VI) occurred in acidic conditions and electrostatic attraction played an important role in  
 346 binding Cr(VI) from the solution. Furthermore, anion exchange between  $Cr^{6+}$  oxyanions and  $Cl^-$  (Khitous et al. 2016)  
 347 on the MSS25 did occur.

348 It can be observed for the EDS result in Fig. 2e (before adsorption) and Fig. 2f (after adsorption) that  $Cl^-$  was  
 349 replaced by  $Cr^{6+}$ . The XRD patterns of MSS25 after adsorption revealed the changes in the MSS25 crystal structure.  
 350 These results indicated that the  $CO_3^{2-}$  groups and carbonate-like species in  $CaCO_3$  were replaced by anionic Cr(VI)  
 351 species ( $CrO_4^{2-}$ ). Moreover, Cr(VI) could be reduced to Cr(III) with the assistance of  $\pi$  electrons on the carboxyl  
 352 groups of MSS25 (peak of 1790 and 1078  $cm^{-1}$  in the FTIR result; see Fig. 3). Electrostatic repulsion between the

353 protonated hydroxyl groups occurred. Cr(III) cations was then adsorbed on MSS25 surface through substitution of  
354  $\text{Fe}^{3+}$  with  $\text{Cr}^{3+}$  in the acidic state, complexation and formation of  $\text{Cr}(\text{OH})_3$  (Zhou et al. 2018). The reduction of Cr(VI)  
355 to Cr(III) in acidic conditions through equations (8) and (9) written below. XRD data of MSS25-Cr also confirmed  
356 that a crystal structure formed after the reaction process with Cr(VI). Cr(VI) might also be adsorbed through the  
357 charge imbalance, vacancies, and generation of chemical bonds due to the magnetic  $\text{Fe}_3\text{O}_4$  on the surface of MSS25:



360

#### 361 **4. Conclusion**

362

363 Magnetic snail shell (MSS25) is a promising adsorbent for removing Cr(VI) from aqueous solutions due to its low  
364 cost and good performance. MSS25 was prepared by a simple process and the adsorption process reached a fast  
365 equilibrium at 150 min. In this study, the MSS25's adsorption capacity of Cr(VI) reached its peak in acidic  
366 conditions at pH of 2-3. The physico-chemical properties data indicated that  $\text{CaCO}_3$  and  $\text{Fe}_3\text{O}_4$  were distributed  
367 uniformly on the MSS25 surface. Our results demonstrated that the maximum adsorption capacity of Cr(VI) by  
368 MSS25 significantly increased after magnetization and the Langmuir maximum adsorption capacity of MSS25 was  
369 46.08 mg Cr(VI)/g MSS25 at initial Cr(VI) concentration of 60 mg/L. The pseudo-second-order model fitted the best  
370 to this study's experimental data. Cr(VI) was adsorbed on MSS25 via ion exchange, electrostatic attraction and  
371 adsorption-coupled reduction. The highly efficient removal of Cr(VI) by MSS25 were helped by large amounts of  
372  $\text{CaCO}_3$  and  $\text{Fe}_3\text{O}_4$  on MSS25.

373

#### 374 **Acknowledgments**

375 The authors would like to acknowledge the financial support given by Thai Nguyen University of Technology  
376 (TNUT) and Thai Nguyen University under grant number DH2019-TN02-04.

377

378

#### 379 **References**

- 380 Akram, M., Bhatti, H. N., Iqbal, M., Noreen, S., & Sadaf, S. (2017). Biocomposite efficiency for Cr(VI) adsorption:  
381 Kinetic, equilibrium and thermodynamics studies. *Journal of Environmental Chemical Engineering*, 5(1), 400–  
382 411. doi:10.1016/j.jece.2016.12.002
- 383 Alidoust, D., Kawahigashi, M., Yoshizawa, S., Sumida, H., & Watanabe, M. (2015). Mechanism of cadmium  
384 biosorption from aqueous solutions using calcined oyster shells. *Journal of Environmental Management*, 150,  
385 103–110. doi:10.1016/j.jenvman.2014.10.032
- 386 An, Q., Li, X. Q., Nan, H. Y., Yu, Y., & Jiang, J. N. (2018). The potential adsorption mechanism of the biochars  
387 with different modification processes to Cr(VI). *Environmental Science and Pollution Research*, 25(31),  
388 31346–31357. doi:10.1007/s11356-018-3107-7
- 389 Bai R, S., & Abraham, T. E. (2001). Biosorption of Cr (VI) from aqueous solution by *Rhizopus nigricans*.  
390 *Bioresource Technology*, 79(1), 73–81. doi:https://doi.org/10.1016/S0960-8524(00)00107-3
- 391 Bhaumik, M., Setshedi, K., & Maity, A. (2013). Chromium (VI) removal from water using fixed bed column of



392 polypyrrole/Fe<sub>3</sub>O<sub>4</sub> nanocomposite. *Separation and Purification Technology*. doi:10.1016/j.seppur.2013.02.037

393 Chen, Y., Wang, B., Xin, J., Sun, P., & Wu, D. (2018). Adsorption behavior and mechanism of Cr(VI) by modified

394 biochar derived from *Enteromorpha prolifera*. *Ecotoxicology and Environmental Safety*, 164, 440–447.

395 doi:<https://doi.org/10.1016/j.ecoenv.2018.08.024>

396 Deveci, H., & Kar, Y. (2013). Adsorption of hexavalent chromium from aqueous solutions by bio-chars obtained

397 during biomass pyrolysis. *Journal of Industrial and Engineering Chemistry*, 19(1), 190–196.

398 doi:10.1016/j.jiec.2012.08.001

399 Dönmez, G., & Aksu, Z. (2002). Removal of chromium(VI) from saline wastewaters by *Dunaliella* species. *Process*

400 *Biochemistry*, 38(5), 751-762 doi:10.1016/S0032-9592(02)00204-2

401 Du, Y., Lian, F., & Zhu, L. (2011). Biosorption of divalent Pb, Cd and Zn on aragonite and calcite mollusk shells.

402 *Environmental Pollution*, 159(7), 1763-1768. doi:10.1016/j.envpol.2011.04.017

403 Ertugay, N., & Bayhan, Y. K. (2008). Biosorption of Cr (VI) from aqueous solutions by biomass of *Agaricus*

404 *bisporus*. *Journal of Hazardous Materials*, 154(1-3), 432-439.

405 doi:10.1016/j.jhazmat.2007.10.070

406 Gong, R., Ding, Y., Liu, H., Chen, Q., & Liu, Z. (2005). Lead biosorption and desorption by intact and pretreated

407 *spirulina maxima* biomass. *Chemosphere*, 58(1), 125-130, doi:10.1016/j.chemosphere.2004.08.055

408 Han, Y., Cao, X., Ouyang, X., Sohi, S. P., & Chen, J. (2016). Adsorption kinetics of magnetic biochar derived from

409 peanut hull on removal of Cr (VI) from aqueous solution: Effects of production conditions and particle size.

410 *Chemosphere*, 145, 336–341. doi:10.1016/j.chemosphere.2015.11.050

411 Hao, Z., Wang, C., Yan, Z., Jiang, H., & Xu, H. (2018). Magnetic particles modification of coconut shell-derived

412 activated carbon and biochar for effective removal of phenol from water. *Chemosphere*, 211, 962-969.

413 doi:10.1016/j.chemosphere.2018.08.038

414 He, R., Peng, Z., Lyu, H., Huang, H., Nan, Q., & Tang, J. (2018). Synthesis and characterization of an iron-

415 impregnated biochar for aqueous arsenic removal. *Science of the Total Environment*, 612, 1177–1186.

416 doi:10.1016/j.scitotenv.2017.09.016

417 Hossain, A., & Aditya, G. (2013). Cadmium biosorption potential of shell dust of the fresh water invasive snail

418 *Physa acuta*. *Journal of Environmental Chemical Engineering*, 1(3), 574-580. doi:10.1016/j.jece.2013.06.030

419 Hossain, A., Bhattacharyya, S. R., & Aditya, G. (2015). Biosorption of cadmium from aqueous solution by shell dust

420 of the freshwater snail *Lymnaea luteola*. *Environmental Technology & Innovation*, 4, 82–91.

421 doi:<https://doi.org/10.1016/j.eti.2015.05.001>

422 Hu, X., Xu, J., Wu, M., Xing, J., Bi, W., Wang, K., et al. (2017). Effects of biomass pre-pyrolysis and pyrolysis

423 temperature on magnetic biochar properties. *Journal of Analytical and Applied Pyrolysis*, 127, 196-202.

424 doi:10.1016/j.jaap.2017.08.006

425 Huu Tap Van, Lan Huong Nguyen, Van Dang Nguyen, X. H. N., Thanh Hai Nguyen, Tien Vinh Nguyen,

426 Saravanamuth Vigneswaran, J. R., & Tran, H. N. (2018). Characteristics and mechanisms of cadmium

427 adsorption onto biogenic aragonite shells-derived biosorbent: Batch and column studies. *Journal of*

428 *Environmental Management*, 241, 535-548. doi.org/10.1016/j.jenvman.2018.09.079

429 Inyang, M. I., Gao, B., Yao, Y., Xue, Y., Zimmerman, A., Mosa, A., et al. (2016). A review of biochar as a low-cost

430 adsorbent for aqueous heavy metal removal. *Critical Reviews in Environmental Science and Technology*,

431 46(4), 406–433. doi:10.1080/10643389.2015.1096880

432 Karimi, M., Shojaei, A., Nematollahzadeh, A., & Abdekhodaie, M. J. (2012). Column study of Cr (VI) adsorption  
433 onto modified silica–polyacrylamide microspheres composite. *Chemical Engineering Journal*, 210, 280–288.  
434 doi:<https://doi.org/10.1016/j.cej.2012.08.046>

435 Khitous, M., Salem, Z., & Halliche, D. (2016). Effect of interlayer anions on chromium removal using Mg–Al  
436 layered double hydroxides: Kinetic, equilibrium and thermodynamic studies. *Chinese Journal of Chemical  
437 Engineering*, 24(4), 433–445. doi:<https://doi.org/10.1016/j.cjche.2015.11.018>

438 Lu, J., Fu, F., Zhang, L., & Tang, B. (2018). Insight into efficient co-removal of Se(IV) and Cr(VI) by magnetic  
439 mesoporous carbon microspheres: Performance and mechanism. *Chemical Engineering Journal*, 346, 590–  
440 599. doi:<https://doi.org/10.1016/j.cej.2018.04.077>

441 Mthombeni, N. H., Mbakop, S., Ray, S. C., Leswifi, T., Ochieng, A., & Onyango, M. S. (2018). Highly efficient  
442 removal of chromium (VI) through adsorption and reduction: A column dynamic study using magnetized  
443 natural zeolite-polypyrrole composite. *Journal of Environmental Chemical Engineering*, 6(4), 4008–4017.  
444 doi:10.1016/j.jece.2018.05.038

445 Mthombeni, N. H., Onyango, M. S., & Aoyi, O. (2015). Adsorption of hexavalent chromium onto magnetic natural  
446 zeolite-polymer composite. *Journal of the Taiwan Institute of Chemical Engineers*, 50, 242–251.  
447 doi:10.1016/j.jtice.2014.12.037

448 Nan, Z., Shi, Z., Yan, B., Guo, R., & Hou, W. (2008). A novel morphology of aragonite and an abnormal polymorph  
449 transformation from calcite to aragonite with PAM and CTAB as additives. *Journal of Colloid and Interface  
450 Science*, 317(1), 77–82. doi:<https://doi.org/10.1016/j.jcis.2007.09.015>

451 Nguyen, L. H., Minh, T., Nguyen, P., Van, H. T., & Vu, X. H. (2019). Treatment of Hexavalent Chromium  
452 Contaminated Wastewater Using Activated Carbon Derived from Coconut Shell Loaded by Silver  
453 Nanoparticles : Batch Experiment. *Water, Air & Soil Pollution*, 230, 68. doi:<https://doi.org/10.1007/s11270-019-4119-8>

454 Rai, M. K., Shahi, G., Meena, V., Meena, R., Chakraborty, S., Singh, R. S., & Rai, B. N. (2016). Removal of  
455 hexavalent chromium Cr (VI) using activated carbon prepared from mango kernel activated with H<sub>3</sub>PO<sub>4</sub>.  
456 *Resource-Efficient Technologies*, 2, S63–S70. doi:<https://doi.org/10.1016/j.reffit.2016.11.011>

457 Saha, P. Das, Dey, A., & Marik, P. (2012). Batch removal of chromium (VI) from aqueous solutions using wheat  
458 shell as adsorbent: process optimization using response surface methodology. *Desalination and Water  
459 Treatment*, 39(1-3), 95–102. doi:10.5004/dwt.2012.2905

460 Shang, J., Pi, J., Zong, M., Wang, Y., Li, W., & Liao, Q. (2016). Chromium removal using magnetic biochar derived  
461 from herb-residue. *Journal of the Taiwan Institute of Chemical Engineers*, 68, 289–294.  
462 doi:<https://doi.org/10.1016/j.jtice.2016.09.012>

463 Tizo, M. S., Blanco, L. A. V., Cagas, A. C. Q., Dela Cruz, B. R. B., Encoy, J. C., Gunting, J. V., et al. (2018).  
464 Efficiency of calcium carbonate from eggshells as an adsorbent for cadmium removal in aqueous solution.  
465 *Sustainable Environment Research*, 28(6), 326–332. doi:<https://doi.org/10.1016/j.serj.2018.09.002>

466 Turan, P., Doğan, M., & Alkan, M. (2007). Uptake of trivalent chromium ions from aqueous solutions using  
467 kaolinite. *Journal of Hazardous Materials*, 148(1–2), 56–63. doi:10.1016/j.jhazmat.2007.02.007

468 Wang, S., Tang, Y., Li, K., Mo, Y., Li, H., & Gu, Z. (2014). Combined performance of biochar sorption and  
469 magnetic separation processes for treatment of chromium-contained electroplating wastewater. *Bioresource*

470 *Technology*, 174, 67–73. doi:<https://doi.org/10.1016/j.biortech.2014.10.007>

471 Wang, X. S., Chen, L. F., Li, F. Y., Chen, K. L., Wan, W. Y., & Tang, Y. J. (2010). Removal of Cr (VI) with wheat-  
472 residue derived black carbon: Reaction mechanism and adsorption performance. *Journal of Hazardous*  
473 *Materials*, 175(1–3), 816–822. doi:10.1016/j.jhazmat.2009.10.082

474 Wang, X. S., Li, Z. Z., & Tao, S. R. (2009). Removal of chromium (VI) from aqueous solution using walnut hull.  
475 *Journal of Environmental Management*, 90(2), 721–729. doi:<https://doi.org/10.1016/j.jenvman.2008.01.011>

476 Xu, J., Yin, Y., Tan, Z., Wang, B., Guo, X., Li, X., & Liu, J. (2019). Enhanced removal of Cr(VI) by biochar with Fe  
477 as electron shuttles. *Journal of Environmental Sciences*, 78, 109–117.  
478 doi:<https://doi.org/10.1016/j.jes.2018.07.009>

479 Yang, Y., Chen, N., Feng, C., Li, M., & Gao, Y. (2018). Chromium removal using a magnetic corncob  
480 biochar/polypyrrole composite by adsorption combined with reduction: Reaction pathway and contribution  
481 degree. *Colloids and Surfaces A: Physicochemical and Engineering Aspects*, 556, 201–209.  
482 doi:<https://doi.org/10.1016/j.colsurfa.2018.08.035>

483 Yuan, P., Fan, M., Yang, D., He, H., Liu, D., Yuan, A., et al. (2009). Montmorillonite-supported magnetite  
484 nanoparticles for the removal of hexavalent chromium [Cr(VI)] from aqueous solutions. *Journal of Hazardous*  
485 *Materials*, 166(2-3), 821-829. doi:10.1016/j.jhazmat.2008.11.083

486 Zhang, X., Zhang, L., & Li, A. (2018). Eucalyptus sawdust derived biochar generated by combining the  
487 hydrothermal carbonization and low concentration KOH modification for hexavalent chromium removal.  
488 *Journal of Environmental Management*, 206, 989–998. doi:10.1016/j.jenvman.2017.11.079

489 Zhao, B., Zhang, J. E., Yan, W., Kang, X., Cheng, C., & Ouyang, Y. (2016). Removal of cadmium from aqueous  
490 solution using waste shells of golden apple snail. *Desalination and Water Treatment*, 57(50), 23987–24003.  
491 doi:10.1080/19443994.2016.1140078

492 Zhou, L., Liu, Y., Liu, S., Yin, Y., Zeng, G., Tan, X., et al. (2016). Investigation of the adsorption-reduction  
493 mechanisms of hexavalent chromium by ramie biochars of different pyrolytic temperatures. *Bioresource*  
494 *Technology*, 218, 351–359. doi:<https://doi.org/10.1016/j.biortech.2016.06.102>

495 Zhou, X., Liu, Y., Zhou, J., Guo, J., Ren, J., & Zhou, F. (2018). Efficient removal of lead from aqueous solution by  
496 urea-functionalized magnetic biochar: Preparation, characterization and mechanism study. *Journal of the*  
497 *Taiwan Institute of Chemical Engineers*, 91, 457–467. doi:<https://doi.org/10.1016/j.jtice.2018.04.018>